LAWRENCE
LIVERMORE
NATIONAL
LABORATORY

UCRL-JRNL-226433

Characterization of bubble core and cloudiness in Yb3+:Sr5(PO4)3F crystals using Micro-Raman spectroscopy

Y. Cui, U. N. Roy, L. Bai, A. Burger, S. R. Qiu, K. Schaffers

November 29, 2006

Journal of Applied Physics

Updated October 14, 2003

Characterization of bubble core and cloudiness in Yb^{3+}:$Sr_5(PO_4)_3F$ crystals using Micro-Raman spectroscopy

Yunlong Cui, Utpal N. Roy, Lihua Bai, and Arnold Burger

Physics Department, Fisk University, Nashville, Tennessee 37208

S. Roger Qiu and Kathleen Schaffers

Lawrence Livermore National Laboratory, Livermore, California 94551

ABSTRACT

Ytterbium doped strontium fluoroapatite Yb^{3+}:$Sr_5(PO_4)_3F$ (Yb: S-FAP) crystals have been used in High Average Power Laser systems as gain medium. Growth induced defects associated with the crystal often affect their performance. In order to improve the crystal quality and its optical applications, it is imperative to understand the nature of these defects. In this study, we utilize Micro-Raman spectroscopy to characterize two common growth-induced defects: bubble core and cloudiness. We find the bubble core consist of voids and microcrystals of Yb: S-FAP. These microcrystals have very different orientation from that of the pure crystal outside the bubble core. In contrast to a previous report, neither $Sr_3(PO_4)_2$ nor Yb_2O_3 are observed in the bubble core regions. On the other hand, the cloudy regions are made up of the host materials blended with a structural deformation along with impurities which include $CaCO_3$, $YbPO_4$, $SrHPO_4$ and $Sr_2P_2O_7$. The impurities are randomly distributed in the cloudy regions. This analysis is necessary for understanding and eliminating these growth defects in Yb:S-FAP crystals.

I. INTRODUCTION

Yb: S-FAP [Yb^{3+}:$Sr_5(PO_4)_3F$] crystals are being used as the gain medium for a 100 J, 10 Hz diode-pumped laser system operating at 1047 nm [1]. Currently 7.0 cm diameter crystals are being routinely grown that yield two laser slabs of dimension 4 x 6 x 0.75 cm^3. However, there are several issues that can affect the yield of suitable crystals [2]. In this research, cloudiness and bubble core have been studied to determine their composition and origin. It is imperative to fully understand these defects in order to eliminate them and produce higher quality laser slabs.

Raman spectroscopy is regarded as a sensitive technique for structural studies and has been utilized to investigate the structure of S-FAP bulk crystals as well as their structural analogs such as $Ca_5(PO_4)_3F$, $Ba_5(PO_4)_3F$, and $Ca_5(PO_4)_3OH$ [3-8]. Furthermore, Confocal micro-Raman spectroscopy is a method developed for the study of materials in a localized space (~ excitation wavelength cubed), and it is an ideal tool to characterize and further identify the origin of the bubble core and cloudiness. In this paper we show the first-order orientation-dependent Raman spectra of bulk Yb: S-FAP crystals and analyze them using group theory. We compare the Raman spectral features in regions free of defects with the spectra at regions containing bubble core and cloudiness, and provide assignments for the additional vibrational peaks.

II. GROUP THEORY ANALYSIS

S-FAP crystallizes with a hexagonal structure [space group $P6_3/m$ (C_{6h}^2), Z = 2]. The elementary cell contains two formula units. Its crystal structure has been described elsewhere [9]. The cell contains six PO_4^{3-} groups with C_s symmetry and two F^- with C_{3h} symmetry. The ten divalent Sr^{2+} ions in the cell occupy two different crystallographic sites. Site I has four Sr^{2+} ions with C_3 symmetry. Site II has six Sr^{2+} ions with C_s symmetry. Although the Yb^{3+} dopant has a strong

tendency to sit in C_s symmetry site, the substitution of the site I may occur and lead to an anomalous absorption [9]. Table 1 gives the site symmetries of an S-FAP crystal and their irreducible representations. The method given in the Ref. 10 was used to calculate all the vibration modes, which were divided into two types, external and internal modes. The external modes include lattice vibrations of the PO_4^{3-}, Sr^{2+} and F^- ions, and the rotations of PO_4^{3-}, which always appear in the low frequency range. The internal modes are PO_4^{3-} modes split by the crystal field. An isolated PO_4^{3-} ion has T_d symmetry and four normal modes of vibration denoted as $A_1(\nu_1)$, $E(\nu_2)$, $T_2(\nu_3)$ and $T_2(\nu_4)$. The effect of the crystal field of the S-FAP lattice on the internal vibrational modes results in breaking their degenerations. The degree of mode splitting depends on the strength of crystal field. [7] Totally, there are 33 ($12A_g+8E_{1g}+13E_{2g}$) Raman-active modes, 20($8A_u+12E_{1u}$) IR -active modes, 29($12B_u+9B_g+8E_{2u}$) inactive (silent) modes and 2 (A_u+E_{1u}) acoustic modes.

In this paper, Raman spectra were collected from the Yb: S-FAP crystals that are mounted in three different orientations. The Y- and Z-axes are identical to the crystallographic a- and c-axes. For the first orientation, Z(Y, *)Z, the crystal c- and a-axis were set to parallel the laser travel and polarization directions, and the scattered Raman signal was collected at a 180° backscattering direction without application of a polarizer. The polarization direction of the Raman signal, denoted as *, was a combination of all possible directions perpendicular to the travel direction of the Raman signal. The polarization directions of laser were set to X and a combination of X and Y by rotating the crystal, however, the corresponding Raman spectra resulted almost identical. In other words, the Raman spectra were the same irrespective to the polarization direction of laser, meaning the a- and b- axes are equivalent. For this orientation, the Raman E_{1g} mode is not predicted by group theory to be observed. For the second orientation, Y (Z, *)Y, laser light

travels in the Y direction and is polarized in the Z direction, Raman signal is collected in the Y direction without application of a polarizer, and no E_{2g} mode is predicted to be observed. In the same way, for the third orientation, Y(X, *)Y, the laser travels in the Y direction and is polarized in the X direction, and all the three A_g, E_{1g} and E_{2g} modes are expected to be observed.

III. EXPERIMENT

Yb:S-FAP crystals were grown by the Czochralski method in a high temperature oxide-type furnace. $SrHPO_4$, $SrCO_3$ and Yb_2O_3 were mixed and melted in the crucible before SrF_2 were added. Yb-doping level was around 1.3×10^{19} ions/cm^3, which is equivalent to 0.1% Sr^{2+} ions in the site II were replaced by Yb^{3+}. The Yb:S-FAP samples examined were labeled C3050202 with bubble core defects, and C171009 with cloudiness. Both a- and c- axes were identified for the crystals. Details of the crystal growth have been reported elsewhere [2].

Raman spectra ranging from 50 to 4500 cm^{-1} were collected by a JOBIN-YVON micro-Raman system in backscattering geometry and confocal configuration. A 632.8 nm, 11 mW He-Ne laser, with no density filter, was used as the light source. A 100× microscopic objective with numerical aperture of 0.9 was used to focus the laser beam onto regions of defects. The spatial resolution was less than 2 μm, and the spectral resolution was 1 cm^{-1}. All the measurements were conducted at room temperature, and the typical acquisition time per spectrum was 10 seconds.

IV. RESULTS AND DISCUSSION

The Raman spectra features of the defect-free Yb:S-FAP crystals strongly depend on the orientation of the crystal relative to the laser travel and polarization directions. Figure 1 presents typical Raman spectra of the sample C3050202 in a region which is far away from bubble core

defects. From top to bottom, Raman spectra in Fig. 1 were obtained in the crystal mounted in three orientations, Z(Y, *)Z, Y(X, *)Y and Y(Z, *)Y, respectively. The external modes are given in the left column of Fig. 1a. The split modes from $A_1(\nu_1)$ and $E(\nu_2)$ are shown in the right and middle columns of the figure. Raman internal modes derived from $T_2(\nu_3)$ and $T_2(\nu_4)$ are given in Fig. 1b. All $15(6A_g+3E_{1g}+6E_{2g})$ internal Raman modes and external Raman modes at 173, 186, 196, 207, 229, 241 and 305 cm^{-1} were observed and identified. Three more peaks at $100(E_{2g})$, $116(A_g)$ and $144(E_{2g})$ cm^{-1} were observed in the anti-Stokes region of Raman spectra. There is an uncertainty to the external mode assignments because modes below 100 cm^{-1} frequency could not be observed due to limitations of the instrumentation.

The Yb^{3+} dopant concentration is so low (~0.1%) that the crystal field of S-FAP is not altered significantly by its ions, therefore, it was not expected to see much difference between the spectra of Yb:S-FAP and S-FAP. If the Yb^{3+} concentration would be increased dramatically, the symmetry of the Sr^{2+} will be changed and the number of external modes, the peak positions, and the intensities associated with the Sr^{2+} ions would be changed as well.

Inside the crystal C3050202, there are many bubble core defects roughly parallel to the c-axis. Figure 2(a) shows a typical optical image of a bubble core defect. The diameter of the core was about 15 μm. It should note that the material inside the bubble has been previously specified as a mixture of $Sr_3(PO_4)_2$ and Yb_2O_3.[2] The $Sr_3(PO_4)_2$ crystal has a trigonal structure [space group $R\bar{3}m$ (D_{3d}^5)], with Raman peaks reported at 143, 173, 217, 245, 417, 572, 622, 955, 998 and 1073 cm^{-1} [11]. However, if $Sr_3(PO_4)_2$ is presented in the region, the peaks at 417 and 572 cm^{-1} would have been observed in Figure 2(b) since they are strong in intensity and far away from those peaks associated with Yb: S-FAP. The absence of these two peaks in Figure 2(b) indicates

that there is no $Sr_3(PO_4)_2$ inside the bubble core. On the other hand, there are new features presented in the spectrum as displayed in Figure 2(b) and we attribute these features to be associated with the E_{1g} modes of S-FAP at 241 and 422 cm^{-1}. However, since the bulk sample was aligned in Z(Y, *)Z orientation, the E_{1g} modes are not supposed to be observable (Figure 1). Therefore there must exist microcrystals of Yb:S-FAP inside the bubble core region, but with a significantly different orientation from the bulk Yb:S-FAP in the defect-free regions.

The Raman spectra collected at the clear region of the sample C171009 crystal is nearly identical to that of sample C3050202 presented in the Fig. 1 but with one exception, that is in the Y(Z, *) Y orientation, the relative intensity of the peak at 445 cm^{-1} (A_g) is lower than that of the peak at 422 cm^{-1} (E_{1g}).

In the cloudy regions there are lots of defects: the whitish inclusions and the precipitate vary in size from 0.5 to 20 μm. If the laser is focused on region free of defects, there is no difference between the spectra collected at these cloudy regions and at other clear regions. However, when the laser is focused on any one of the defect regions, new peaks appear in the spectrum. Figure 3 shows stacked Raman spectra of the sample C171009 collected at the cloudy areas A, B, C, D, E and F. The areas A-F located close to the surfaces of the sample are where we could reach and identify impurities with our Raman system. The Raman spectra collected at a clear area in the Y(X, *) Y orientation is presented at the bottom of the figure for comparison. New peaks collected at these areas and their impurity assignments are given in the Table 2. In area A, the relative weak peak at 1054 cm^{-1} is shifted to 1051 cm^{-1} and enhanced significantly, and a new peak appears at 716 cm^{-1}. In the experiment of laser induced decomposition of KH_2PO_4 crystals [12], new Raman peaks at 1046 and 714 cm^{-1} were observed at surface damage sites. Therefore,

the new feature may be due to a deformation of the PO_4^{3-} group, and results in the formation of a PO_3^- group in certain cases. In area B, three new peaks at 282, 713 and 1087 cm^{-1} were observed; the peak positions and relative intensities are almost the same as those of a $CaCO_3$ crystal [13]. Since calcium contamination had been detected and was present in the $SrCO_3$ starting material [9], the peaks collected at this area might result from a $CaCO_3$ impurity. However, it is worth noting that no Raman signal corresponding to $SrCO_3$ was detected. In area C, two weak peaks at 1003 and 1086 cm^{-1} were observed. The peak at 1005 cm^{-1} is found in $Ca_5(PO_4)_3F$ crystals and is attributed to the $[HPO_4]^{2-}$ center [6]. Therefore, the defect at area C was attributed to a combination of $CaCO_3$ and $[HPO_4]^{2-}$. In area D, peaks at 281, 490, 688, 711, 1002 and 1086 cm^{-1} are observed. Taking into account that the peaks at 499, 678 and 1086 cm^{-1} were observed in the Raman spectra of $TmPO_4$ [14], an isostructural material of $YbPO_4$ [15], we attribute the peaks at 490 and 688 cm^{-1}, and part of the peak at 1086 cm^{-1} to the $YbPO_4$ impurity. In the area E, there are eight new peaks at 281, 435, 567, 714, 907, 985, 996 and 1086 cm^{-1} being found. The Raman peak at 985 cm^{-1} has been reported to be the strongest peak of the spectra collected from $SrHPO_4$ powder, a starting material to grow the S-FAP crystal [2]. In the area F, four new peaks at 290, 385, 734 and 1002 $cm^{-1}$are found, the 734 cm^{-1} peak was the strongest. Since the 741 cm^{-1} peak was associated with the $[P_2O_7]^{4-}$ group [16]; two PO_3^- groups bridged through an oxygen atom, the impurity at the area F might contain $Sr_2P_2O_7$.

In summary, we find the bubble core region consists of voids with microcrystals of Yb: S-FAP but with different orientation than the bulk material. In the cloudy regions, several types of impurities are identified and these impurities are distributed randomly in the cloudy region. The identification of the compounds inside the bubble core and cloudy regions may lead to improvement of Y-SFAP quality and its optical application.

ACKNOWLEDGEMENTS

The authors at Fisk University gratefully acknowledge financial support from the LLNL Research Collaborations Program fro HBCUs and MIs and from the NSF-supported Center of Research Excellence in Science and Technology (CREST, Cooperative Agreement CA-0420516). The authors also thank Dr. Enrique Silberman for his valuable suggestions. This work was performed under the auspices of the U.S. Department of Energy by University of California, Lawrence Livermore National Laboratory under contract No. W-7405-Eng-48.

Figure captions:

Fig. 1a. Raman spectra of a Yb^{3+}:$Sr_5(PO_4)_3F$ crystal in the regions of external modes (left column), and of the internal modes E(ν_2) (middle column) and A(ν_1) (right column) modes.

Fig. 1b. Raman spectra of a Yb^{3+}:$Sr_5(PO_4)_3F$ crystal in the regions of modes derived from the $T_2(\nu_4)$ (left column) and $T_2(\nu_3)$ (right column) vibrations.

Fig. 2a. Micrograph of a bubble core defect in the C3050202 crystal. Raman signals were collected at the center of the core, and around 25 μm away from it.

Fig. 2b. Raman spectra collected inside and outside a bubble core defect of the sample C3050202.

Fig.3 Stacked Raman spectra of the sample C171009 at the cloudy areas A, B, C, D, E and F. The spectrum collected at clear area in Y(X, *)Y orientation is presented at the bottom for comparison.

REFERENCE

1. C. D. Orth, S. A. Payne, and W. F. Krupke, Nucl. Fusion 36, 75(1996).

2. K.I. Schaffers, J. B. Tassano, A. B. Bayramian, and R.C. Morris, J. Cryst. Growth 253, 297(2003).

3. L.C. Kravitz, J. D. Kingsley, and E. L. Elkin, J. Chem. Phys. 49, 4600(1968).

4. L. L. Boyer and P. A. Fleury, Phys. Rev. B, 2693(1974).

5. H. Tsuda and J. Arends, J. Dent. Res. 73, 1703(1994).

6. G. Leroy, N. Leroy, G. Penel, C. Rey, P. Lafforgue, and E. Bres, Appl. Spectrosc. 54, 1521(2000).

7. C.E. Bonner, C.C. Chess, C. Meegoda, S. Stefanos, and G.B. Loutts, Opt. Mater. 26, 17(2004).

8. P. N. de Aza, F. Guitian, C. Santos, S. de Aza, R. Cusco and L. Artus, Chem. Mater. 9, 916(1997).

9. A. Z. Nelson, T. van Buuren, C. Bostedt, K. I. Schaffers, L. J. Terminello, M. Engelhard, and Don Baer, J. Appl. Phys. 91, 5135(2002).

10. W. G. Fateley, N. T. McDevitt, and F. F. Bentley, Appl.Spectrosc. 25, 155(1971).

11. L. Popovic, B. Manoun, and D. de Waal, J. Alloy. Comp. 343, 82(2002).

12. R. A. Negres, S. O. Kucheyev, P. DeMange, C. Bostedt, T. van Buuren, A. J. Nelson, and S. G. Demos, Appl. Phys. Lett. 86, 171107(2005).

13. H. N. Rutt and J. H. Nicola, J. Phys. C7, 4522(1974).

14.S. Guha, Phys. Rev. B23, 6790(1981).

15. P.C. Becker, G. M. Williams, and N. M. Edelstein, J. A. Koningstein, L.A. Boatner, and M. M. Abraham, Phys. Rev. B45, 5027(1992).

16. B. Manoun, B. E. Bali, S.K. Saxena, and R. P. Gulve, J. Mol. Struct. 794, 334(2006).

Table 1. Atomic group site symmetries and their irreducible representations in $Sr_5(PO_4)_3F$ [space group $P6_3/m$, Z=2] crystal.

Atomic group	Multiplicity	Site symmetry	Irreducible representation
PO_4^{3-}	6	Cs	$2A_g+2E_{2g}+2B_u+2E_{1u}+B_g+E_{1g}+A_u+E_{2u}$
Sr^{2+}	6	Cs	$2A_g+2E_{2g}+2B_u+2E_{1u}+B_g+E_{1g}+A_u+E_{2u}$
Sr^{2+}	4	C_3	$A_g+ B_g +A_u +B_u+E_{1g}+E_{2g}+E_{1u}+E_{2u}$
F^-	2	C_{3h}	$B_g+A_u +E_{1u}+E_{2g}$

Lattice vibrations of the PO_4^{3-}, Sr^{2+}, and F^- ions

$\Gamma_{lat}= 5A_g+3E_{1g}+6E_{2g} +3A_u+5E_{1u}+5B_u+4B_g+3E_{2u}$

Rotations (librations) on the PO_4^{3-} ion

$\Gamma_{rot}= A_g+2E_{1g}+ E_{2g} +2A_u+ E_{1u}+ B_u+ 2B_g+2E_{2u}$

External (intermolecular) vibrations

$\Gamma_{ext}= 6A_g+5E_{1g}+7E_{2g} +5A_u+6E_{1u}+6B_u+6B_g+5E_{2u}$

Internal (intramolecular) vibrations of PO_4^{3-}

$\Gamma_{int}= 6A_g+3E_{1g}+6E_{2g} +3A_u+6E_{1u}+6B_u+3B_g+3E_{2u}$

Modes classification

$\Gamma_{Raman}= 12A_g+8E_{1g}+13E_{2g}$ $\Gamma_{ir}= 8A_u+12E_{1u}$

$\Gamma_{acoustic}= A_u+E_{1u}$ $\Gamma_{silent} =12B_u+9B_g+8E_{2u}$

$A_g \rightarrow \alpha_{xx}+\alpha_{yy}, \alpha_{zz}$ $E_{1g} \rightarrow \alpha_{yz}, \alpha_{zx}$ $E_{2g} \rightarrow \alpha_{xx}-\alpha_{yy}, \alpha_{xy}$

Table 2. New Raman peaks collected at different cloud regions at the C171009 sample and their corresponding defect and impurity assignments.

Region	New peak position (cm^{-1})	Assignment
A	716, 1051	deformation of PO_4^{3-}
B	**282, 713, 1087**	$CaCO_3$
C	*1003*, **1086**	$[HPO_4]^{2-}$, $CaCO_3$
D	**281,** 490, 688**, 711,** *1002***, 1086**	$YbPO_4$, $[HPO_4]^{2-}$, $CaCO_3$
E	**281,** 435, 567, **714,** 907, 985, *996,* **1086**	$SrHPO_4$, $[HPO_4]^{2-}$, $CaCO_3$
F	290, 385, 734, *1002*	$Sr_2P_2O_7$, $[HPO_4]^{2-}$

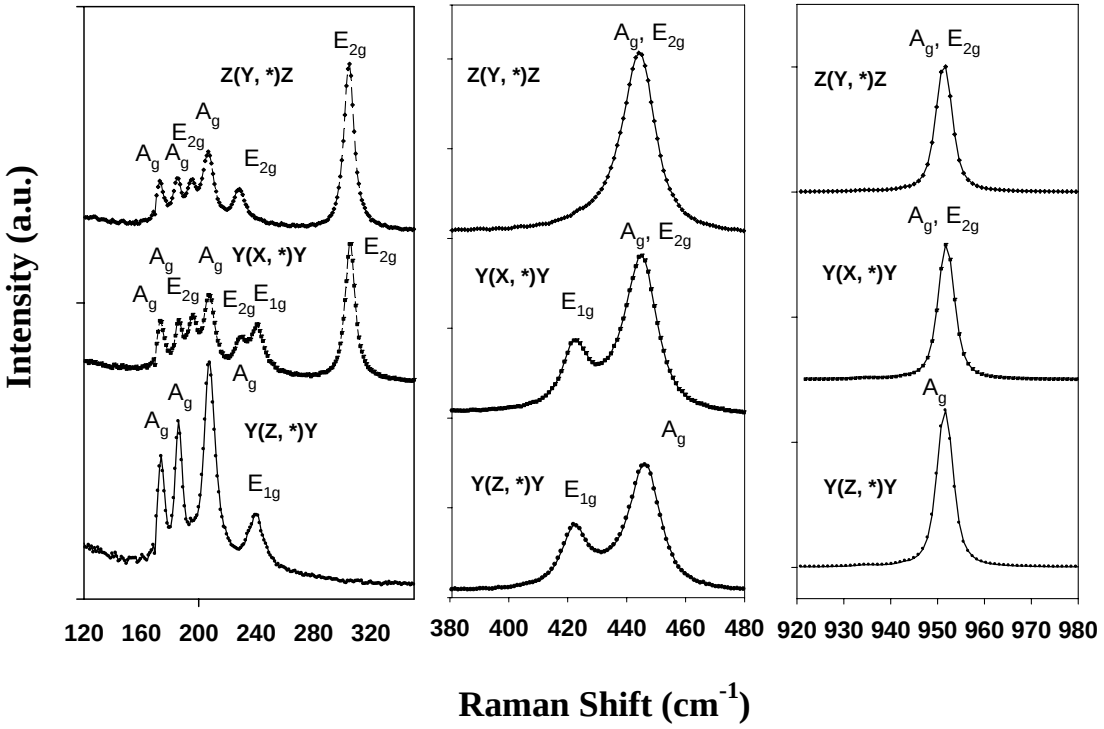

Fig. 1a. Raman spectra of a Yb^{3+}:$Sr_5(PO_4)_3F$ crystal in the regions of external modes (left column), and the internal modes E(ν_2) (middle column) and A(ν_1) (right column).

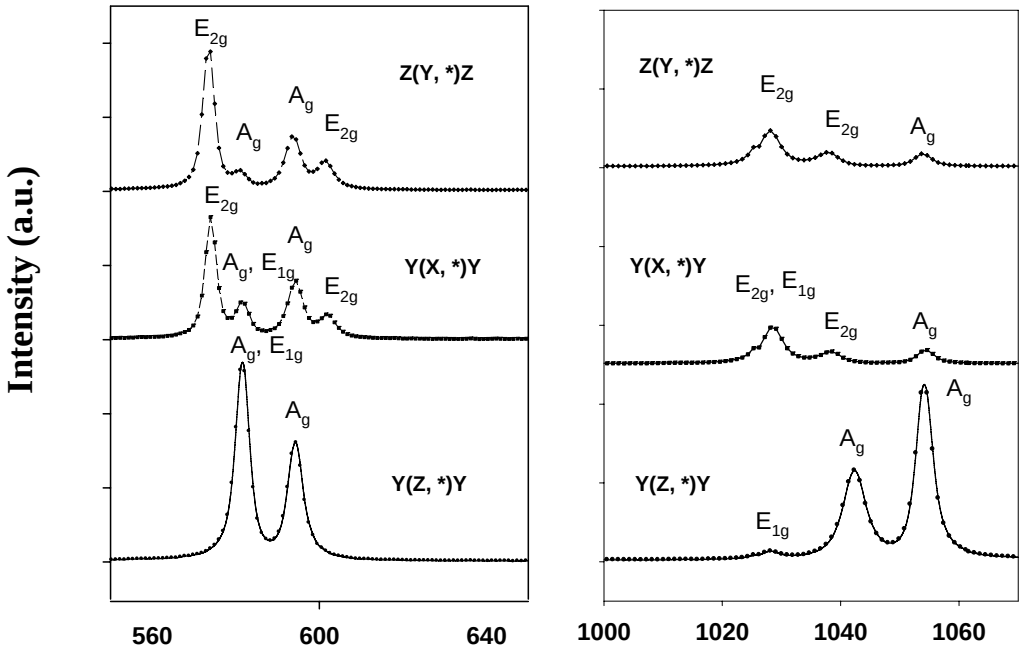

Fig. 1b. Raman spectra of a Yb^{3+}:$Sr_5(PO_4)_3F$ crystal in the regions of modes derived from the $T_2(\nu_4)$ (left column) and $T_2(\nu_3)$ (right column) vibrations.

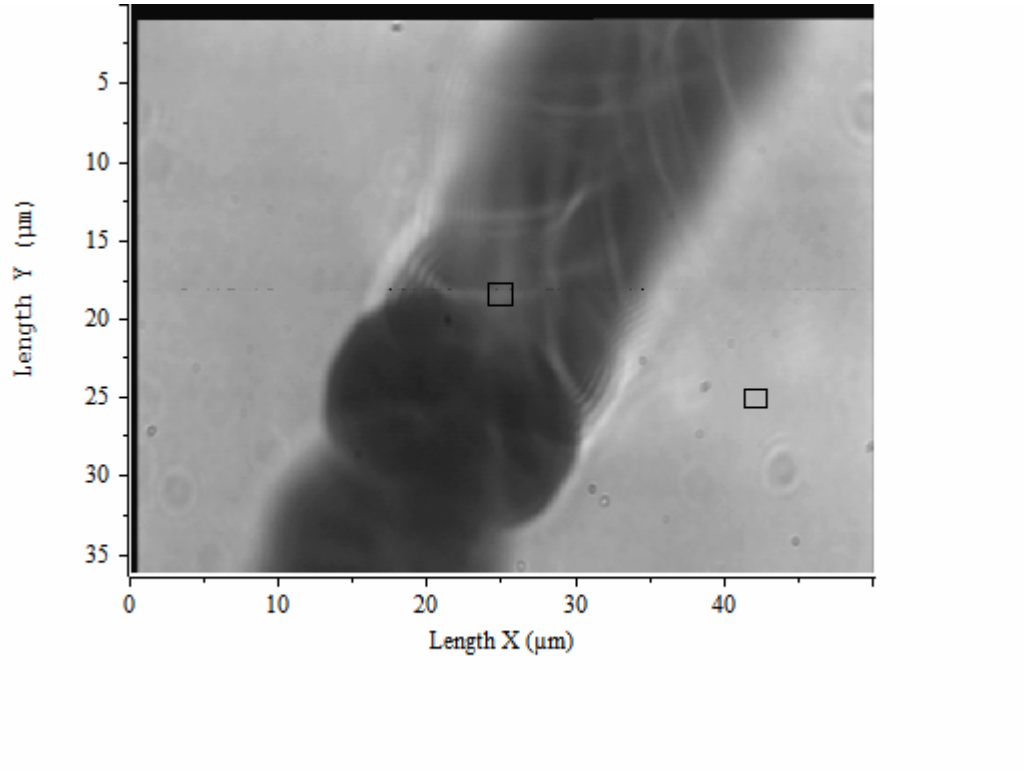

Fig. 2a. Micrograph of a bubble core defect of in the C3050202 crystal. Raman signals were collected at the center of the core, and around 25 µm away from the it.

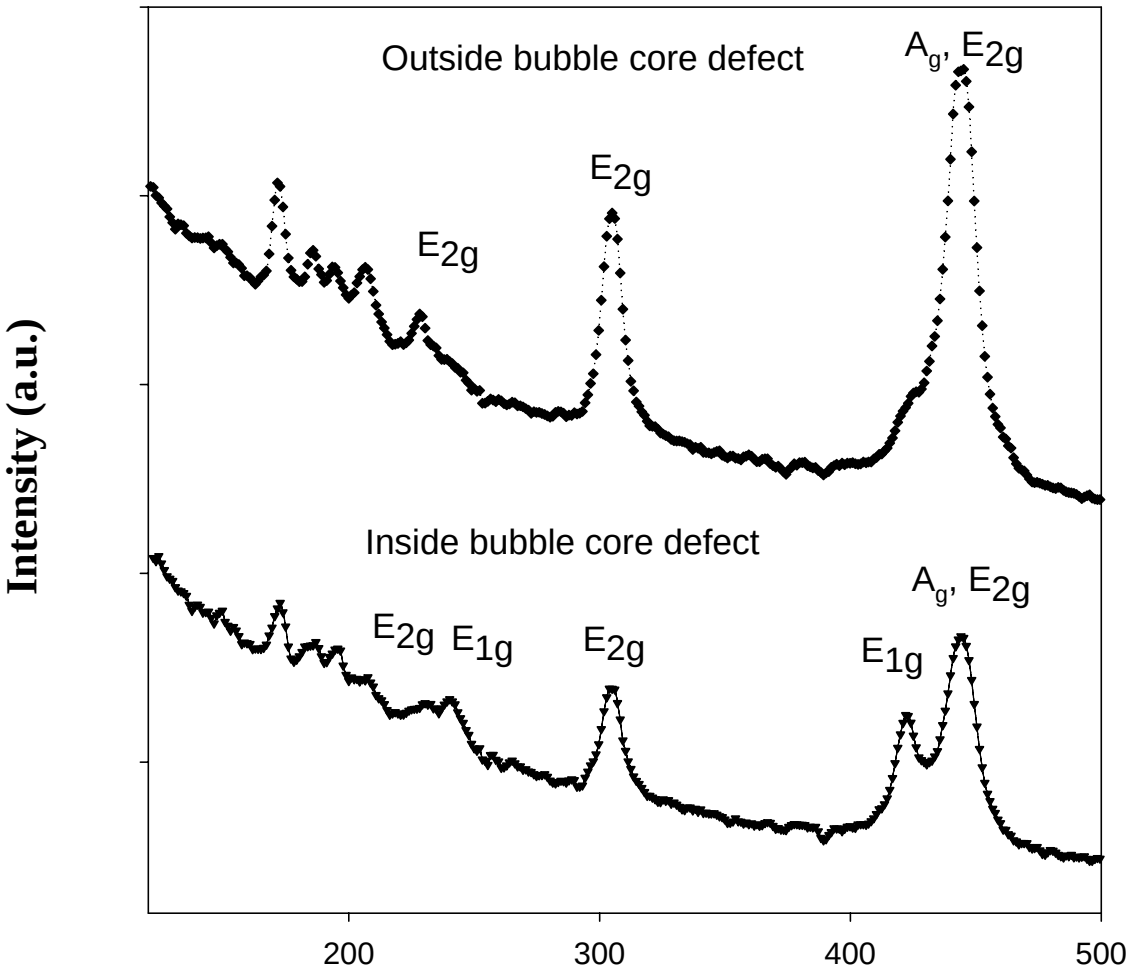

Fig. 2b. Raman spectra collected inside and outside bubble core defect of the sample C3050202.

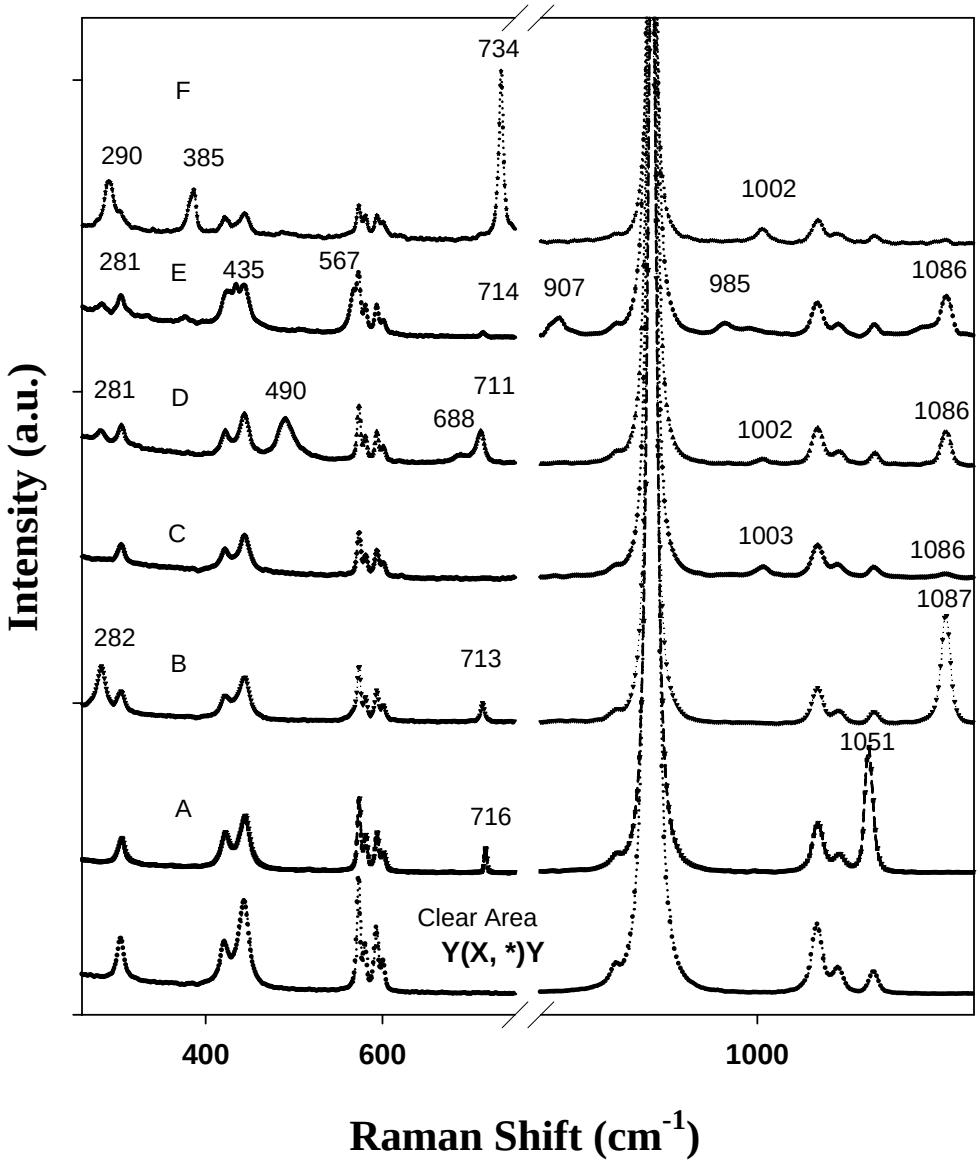

Fig. 3. Stacked Raman spectra of the sample C171009 at the cloudy areas A, B, C, D, E and F. The spectrum collected at a clear area in the Y(X, *)Y orientation is presented at the bottom for comparison.